

LiDAR Based Semantic Perception for Forklifts in Outdoor Environments

Benjamin Serfling*, Hannes Reichert*, Lorenzo Bayerlein, Konrad Doll and Kati Radkhah-Lens

Abstract—In this study, we present a novel LiDAR-based semantic segmentation framework tailored for autonomous forklifts operating in complex outdoor environments. Central to our approach is the integration of a dual LiDAR system, which combines forward-facing and downward-angled LiDAR sensors to enable comprehensive scene understanding, specifically tailored for industrial material handling tasks. The dual configuration improves the detection and segmentation of dynamic and static obstacles with high spatial precision. Using high-resolution 3D point clouds captured from two sensors, our method employs a lightweight yet robust approach that segments the point clouds into safety-critical instance classes such as pedestrians, vehicles, and forklifts, as well as environmental classes such as driveable ground, lanes, and buildings. Experimental validation demonstrates that our approach achieves high segmentation accuracy while satisfying strict runtime requirements, establishing its viability for safety-aware, fully autonomous forklift navigation in dynamic warehouse and yard environments.

I. INTRODUCTION

A. Motivation

Autonomous guided vehicles (AGV) play an increasingly vital role in modern industrial operations. Although compact indoor vehicles, such as pallet lifters and platform AGVs, have achieved a high level of autonomy, larger vehicles, such as counterweight forklifts, still rely heavily on human operators. These forklifts are often required to navigate complex environments that span both indoor and outdoor settings, making full automation considerably more challenging.

One of the key technical hurdles in enabling autonomous forklift operation is semantic perception, including the accurate detection of drivable free space. This capability is fundamental to core tasks such as path planning, task allocation, and collision avoidance. Inaccurate semantic perception can lead to inefficient navigation, increased operational time, and potential safety hazards. It also impacts the vehicle's ability to detect and track obstacles like pedestrians, other vehicles, or dynamic objects. Achieving robust semantic perception in real-world warehouse environments is particularly challenging due to their unstructured nature, characterized by irregular layouts, movable obstacles such as pallets and racks, and the absence of clear lane markings. In addition, forklifts frequently transition between indoor and outdoor areas, where lighting and surface conditions can vary dramatically.

B. Serfling, H. Reichert, K. Doll and K. Radkhah-Lens are with the Faculty of Engineering and Informatics, University of Applied Sciences Aschaffenburg, Aschaffenburg, Germany `firstname.lastname@th-ab.de`

L. Bayerlein is with the Linde Material Handling GmbH, Kion Group, Aschaffenburg, Germany `lorenzo.bayerlein@kiongroup.com`

*The authors contributed equally.

Moreover, automotive-grade sensors, that are designed for narrow fields of view and long-range detection on highways, are not suitable for forklift applications, which require up to 270 ° coverage and accurate short-range detection of objects approaching from the side, especially within tight warehouse aisles. Because no standard solution meets these needs, we propose a custom dual-LiDAR configuration and perception pipeline specifically optimized for the spatial and operational constraints of industrial logistics environments.

The use of rear wheel steering introduces further complications, as high angular velocity can produce motion blur in sensor data, reducing the effectiveness of vision-based methods.

LiDAR is a key technology for autonomous forklift, providing precise 3D perception that remains robust under varying lighting conditions, in contrast to camera-based systems. It enables the accurate detection of free space and obstacles in mixed indoor-outdoor unstructured environments. Recent industry trends indicate increasing LiDAR resolution and decreasing sensor costs, making high-performance LiDAR more accessible and practical for industrial AGV applications. This combination of precision, reliability, and affordability establishes LiDAR as a key enabler for safe and efficient autonomous navigation. However, the deployment of high-resolution LiDAR in real-world warehouse environments remains largely unexplored.

B. Requirements

1) *Real-Time Constraints*: Real-time processing is critical for autonomous forklifts operating in dynamic environments like warehouses. With two Ouster OS0-128 LiDAR sensors running at 10 Hz, each provides a full scan every 100 ms. We target a 30 Hz control loop for perception, allowing 33.3 ms to be allocated to process sensor data. This leaves additional runtime for downstream tasks, such as path planning and decision making.

2) *Segmentation Accuracy*: High segmentation accuracy is critical for safe and reliable autonomous forklift operation. Consistent identification of drivable ground is required for effective path planning, while precise detection of safety-critical classes, especially pedestrians, is essential for collision avoidance and emergency braking. Segmentation performance directly influences the system's ability to make safe navigation decisions and respond to dynamic changes in the environment.

C. Related Work

1) *Automotive LiDAR Semantic Segmentation*: Large-scale annotated datasets such as SemanticKITTI [4], Seman-

ticPOSS [17], SemanticUSL [11], SemanticTHAB [19], nuScenes [6], and the Waymo Open Dataset [22] have significantly advanced LiDAR-based semantic segmentation for autonomous driving. These benchmarks have fostered a variety of approaches aimed at optimizing the trade-off between segmentation accuracy and computational efficiency.

Spherical projection-based methods, such as FRNet [30], FIDNet [32], and CENet [5], convert 3D point clouds into 2D range images, allowing fast inference through convolutional neural networks (CNNs) while preserving competitive mean Intersection over Union (mIoU) scores. More recent Vision Transformer (ViT)-based architectures, including RangeFormer [13] and RangeViT [2], further improve accuracy but at the cost of increased latency and reduced frame rates.

Alternatively, volumetric and raw point cloud-based methods such as SphereFormer [14], Cylinder3D [33], and MinkUNet [24] generally achieve higher segmentation accuracy, but are often unsuitable for real-time deployment due to computational complexity. The current state-of-the-art semantic segmentation accuracy on SemanticKITTI is held by the Point Transformer V3 foundation model [29]. However, as highlighted by Reichert et al. [20], many of these methods struggle to scale to high-resolution LiDAR sensors under strict real-time constraints. Their work introduces a revised spherical projection strategy coupled with a lightweight CNN backbone that enables real-time semantic segmentation of high-resolution scans.

2) *LiDAR-Based Perception in Material Handling*: Material handling perception tasks present a different set of challenges compared to autonomous driving, including unstructured environments, dynamic obstacles, and the need for rapid inference to support agile robotic behavior.

The SeMantic InDUstry dataset [28] targets specifically the industrial domain. However, it is limited to static scene elements and does not include dynamic object classes such as forklifts or persons. Furthermore, the LiDAR sensors used have a low resolution compared to modern standards. The Goose-Ex dataset [7] provides high-resolution annotated LiDAR scans for the operation of an excavator in unstructured outdoor environments.

Schreck et al. [21] addresses the challenges of material handling with a heuristic method for free space detection, tailored to forklifts operating in mixed indoor-outdoor spaces. Their approach uses height-change cues and surface normals computed from spherical projections to segment traversable regions in real time, making it well-suited for cluttered warehouse scenes where dense semantic segmentation may be infeasible.

In addition to this, Gonzalez et al. [3] propose a dual function algorithm that combines human localization and free space segmentation. Using sparse point cloud representations and region-growing techniques, their system reliably identifies navigable ground and potential human obstacles with minimal computational overhead. Designed for deployment on mobile robots in warehouse facilities, their method emphasizes safety and efficiency in real-world industrial environments.

D. Contributions

In the state of the art, various approaches have been presented for LiDAR semantic segmentation. However, all of these methods are developed for road traffic scenarios. Transferring concepts from the traffic domain to industrial warehouse environments remains a challenge and is largely unexplored. In this context, the main contributions of this paper are:

- A method for 3D semantic segmentation using data from a dual-LiDAR setup mounted on a counterbalance forklift.
- An empirical study of LiDAR-based semantic segmentation in real-world industrial warehouse environments.

E. Outline

The remainder of this article is structured as follows: In [section II](#), the dataset and the data collection process are described. Followed by our method for semantic perception in [section III](#). Our results are reported in [section IV](#), followed by a conclusion and short outlook in [section V](#).

II. DATASET



Fig. 1: Prototype forklift in action. © Linde Material Handling

Figure 1 shows the recording system used in action. For our data collection, we utilize the two Ouster OS0-128 LiDAR sensors mounted on the roof [16]. The sensors are synchronized using the precision time protocol (PTP) with GPS time as reference. We recorded our data at the Linde Material Handling factory site during normal work operations. For the annotation process, we utilize *PointLabeler* by J. Behley et al. [4], which supports the grouping and annotation of multiple LiDAR scans through ego motion compensation. To estimate ego-motion, we employ the Ouster SDK SLAM module, which incorporates a high-level implementation of *KISS-ICP* [27]. We collected a total of 7676 LiDAR scans in four sequences with a total of 2012.2 million annotated 3D points. Sequence 0000 is reserved for testing, while the remaining sequences are used for training (see [Table I](#)). Due to the nature of the factory site, we recorded a large number of forklifts and material handling utilities from various perspectives. We defined our classes based on their relevance to

TABLE I: Dataset Scenes

Sequence	Frames	Scans	Points	Split
0000	665	1330	348.6 M	Test
0001	667	1334	349.7 M	Train
0002	723	1446	379.1 M	Train
0003	1783	3566	934.8 M	Train

material handling resulting in the following semantic classes:

TABLE II: Class Definitions

Class	Definition
<i>car</i>	Vehicle designed for road traffic.
<i>forklift</i>	Forklift used for material handling.
<i>person</i>	Human pedestrian.
<i>object</i>	Movable object or temporary obstacle.
<i>driveable ground</i>	Surface suitable for AGV navigation.
<i>other ground</i>	Surface not suitable for AGV navigation.
<i>lane marking</i>	Painted or marked lane indicator on the ground.
<i>vegetation</i>	Natural plant life including grass, shrubs, and trees.
<i>building</i>	Static man-made structure.

The distribution of the classes in our data set can be seen in [Figure 2](#). Note that the figure is using logarithmic scale. We created a reference map of scene 0000 using VDBfusion

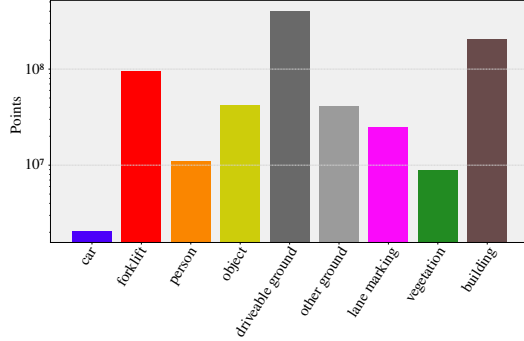


Fig. 2: Distributions of semantic classes in SemanticTHAB.

[\[26\]](#) as shown in [Figure 3](#). We remove all dynamic objects for better visualization.

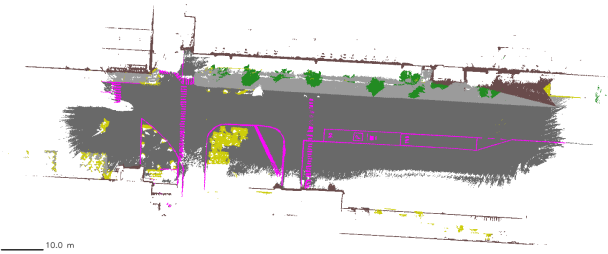


Fig. 3: Reference Map of Scene 0000.

III. METHOD

The following section contains an explanation of the methods used in our perception pipeline. Our method consists

of two main steps. First, our data preparation process is detailed in [subsection III-A](#), which includes structuring the LiDAR point clouds into an image-like format, transforming the scans into a defined forklift coordinate system, and computing surface normals. Second, we present our core semantic segmentation method in [subsection III-B](#).

A. Preprocessing

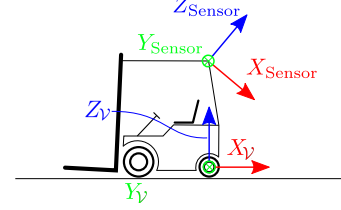


Fig. 4: The forklift vehicle frame (following ISO 8855 conventions) and the LiDAR sensor coordinate frame.

Our method uses a staggered, image-like LiDAR representation based on spherical projection, following [\[18\]](#), [\[20\]](#). Each 3D point $\vec{p} = [x, y, z]^T$ is transformed into spherical coordinates $\vec{x} = [\phi, \theta, r]^T$, where ϕ is the azimuth, θ the inclination, and r the range. These are projected into image coordinates (u, v) using:

$$\begin{bmatrix} u \\ v \\ 1 \end{bmatrix} = \begin{bmatrix} \frac{1}{\Delta\phi} & 0 & c_\phi \\ 0 & \frac{1}{\Delta\theta} & c_\theta \\ 0 & 0 & 1 \end{bmatrix} \cdot \begin{bmatrix} \phi \\ \theta \\ 1 \end{bmatrix} \quad (1)$$

This generates spherical images $I_{x,y,z}(u, v)$, reflectivity maps $I_{ref}(u, v)$ (see [Figure 5](#)), and range images $I_r(u, v)$ via Euclidean norm. In addition, we can transform the semantic annotation $I_{sem}(u, v)$ into a spherical image.

The points in the point cloud and their corresponding pixels are transformed to the vehicle coordinate system \mathcal{V} defined in ISO8855 [\[10\]](#) using a transformation matrix:

$${}^{\mathcal{V}}I_{x,y,z}(u, v) = \begin{bmatrix} R & t \end{bmatrix} I_{x,y,z}(u, v) \quad (2)$$

This transformation is crucial because it assumes that the ground of the immediate surroundings is parallel to the vehicle's xy -plane. The ISO8855 coordinate system defines the center rear wheel axis as the origin and the x axis is aligned with the movement direction as shown in [Figure 4](#). Using a joint coordinate system is essential for the fusion of both LiDAR sensors in our perception approach.

Surface normals provide a local geometric context for segmentation and obstacle detection. Following [\[20\]](#), [\[21\]](#), we estimate normals using finite differences. For each pixel $P_c = {}^{\mathcal{V}}I_{x,y,z}(u, v)$ and its neighbors $P_b = {}^{\mathcal{V}}I_{x,y,z}(u + 1, v)$, $P_a = {}^{\mathcal{V}}I_{x,y,z}(u, v + 1)$, the normal is computed as:

$${}^{\mathcal{V}}I_{n_x, n_y, n_z}(u, v) = \frac{(P_b - P_c) \times (P_a - P_c)}{\|(P_b - P_c) \times (P_a - P_c)\|_2} \quad (3)$$

This produces a dense surface normal map $I_{n_x, n_y, n_z}(u, v)$ for downstream geometric processing. Examples of surface normals can be seen in [Figure 5](#).

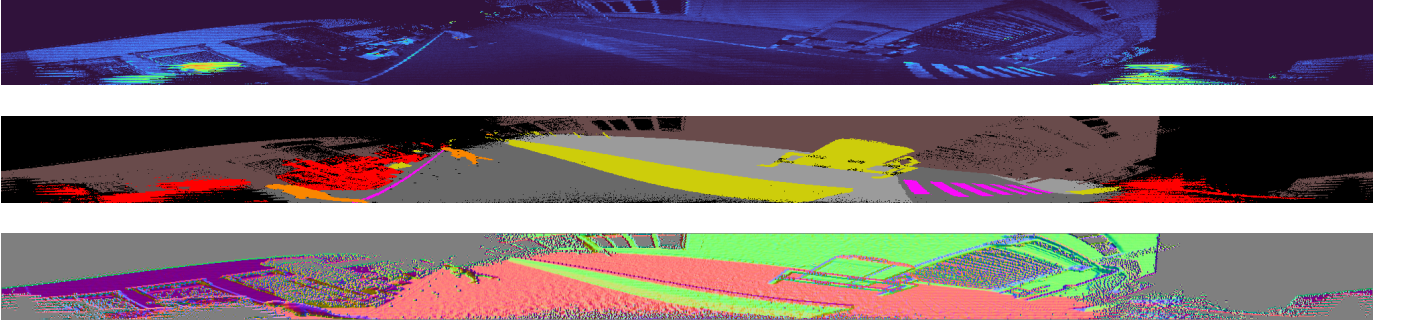


Fig. 5: Spherical projections of reflectivity measurements (top), semantic annotations (middle), and surface normals (bottom)

B. Semantic Segmentation

For our semantic segmentation module, we use CNNs as it is evident from [subsection I-C](#) that CNNs are well suited for real-time processing of spinning LiDAR scans. As input, we utilize the spherical projection of the point cloud expressed in the forklift coordinate system, denoted ${}^v I_{x,y,z}(u,v)$, the reflectivity measurements represented as the spherical image $I_{ref}(u,v)$, and the surface normals ${}^v I_{n_x,n_y,n_z}(u,v)$. We assume that reflectivity measures $I_{ref}(u,v)$ are essential for detecting classes such as *lane markings*, which are visible exclusively in reflectivity data. Furthermore, we assume that ${}^v I_{n_x,n_y,n_z}(u,v)$ enhances the network’s ability to identify structures by leveraging their orientation and homogeneity. We follow the insights of [1] and include ${}^v I_{x,y,z}(u,v)$ and ${}^v I_{n_x,n_y,n_z}(u,v)$ downsized to the respective resolution at any stage where the spatial resolution of the latent feature map changes to improve 3D consistency. For the neck, we first employ multiplicative self-attention [25] by using multi-scale features extracted from the backbone. The attention-weighted features are then upsampled using deconvolution layers to the shape $H/2 \times W/2$ (i. e. 64×1024) and merged by a concatenation operation to build a feature pyramid network (FPN) [15]. FPN enhances the ability of network to detect objects of vastly different sizes by combining low-resolution, semantically strong features with high-resolution, semantically weak features. For the segmentation head, we use a deconvolution layer to reshape the output to $H \times W$ (i. e. 128×2048), followed by two convolutional layers for anti-aliasing. Our network architecture is visualized in [Figure 6](#). As backbones, we support three variants from the *ResNet* family (*ResNet18*, *ResNet34*, and *ResNet50*) [9], as well as three variants from the *ShuffleNet* family [31] and three backbones from the *EfficientNet* family [23].

C. Implementation Details

1) *Training Objectives*: For the loss functions, we use a weighted sum of the cross-entropy loss \mathcal{L}_{CE} and the Tversky loss $\mathcal{L}_{Tversky}$ [8]. The Tversky loss allows for adjusting the balance between false positives and false negatives, which is particularly useful for detecting smaller objects. During training, we treat each of the two sensors separately by

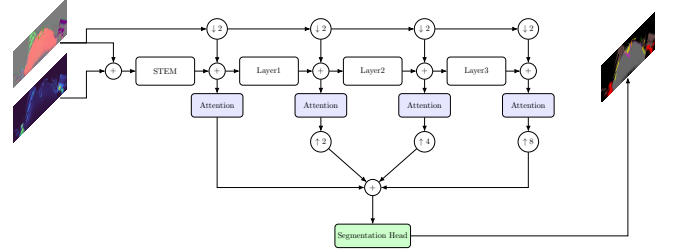


Fig. 6: **Model Architecture**: white blocks indicate the backbone path; \downarrow denotes nearest-neighbor downsampling; $+$ represents feature concatenation; \uparrow corresponds to deconvolution-based upsampling; the green block indicates the segmentation head.

randomly mixing data from both sensors into the training batches.

2) *Training Curriculum*: Our models were trained with a batch size of 8 and a learning rate of 0.001, using the ADAM optimizer [12]. To ensure stable training and convergence, we incorporated a learning rate scheduler. All models were initially pre-trained on the SemanticKITTI dataset for 50 epochs, followed by fine-tuning on our dataset for 30 epochs. We trained our model on all sequences except 0000, which we use for testing.

3) *Hardware Setup*: We use a single Nvidia RTX 3090 for training and testing. If not explicitly stated differently, all run times are measured using a RTX 3090.

4) *Inference*: During inference, we operate our semantic segmentation model with a batch size of two, i. e. one for each LiDAR sensor.

IV. RESULTS

The standard metric for evaluating semantic segmentation is the mean Intersection over Union (mIoU). For each class c , it compares the prediction region with the ground truth region, resulting in

$$IoU_c = \frac{\sum_{u,v} \mathbb{1}(I_{sem}^{Pred}(u,v) = c \wedge I_{sem}^{GT}(u,v) = c)}{\sum_{u,v} \mathbb{1}(I_{sem}^{Pred}(u,v) = c \vee I_{sem}^{GT}(u,v) = c)} \quad (4)$$

with $I_{sem}^{Pred}(u,v)$ being the predicted label, $I_{sem}^{GT}(u,v)$ the ground truth and $\mathbb{1}$ the indicator function. The IoU is averaged over the entire test set and all classes to obtain the mIoU.

TABLE III: **Quantitative Results:** Comparison of different backbones in terms of model size (Parameters), inference time (single and dual), per-class IoU for selected classes, and overall mean IoU (mIoU)

Backbone	Parameters	Inference Time		forklift	person	object	driveable ground	lane marking	building	mIoU
		single	dual							
ResNet18	9.03M	8ms	14ms	85.51	62.50	56.65	92.32	26.87	91.67	69.06
ResNet34	24.27M	12ms	22ms	88.93	73.01	59.77	92.47	39.91	91.58	72.31
ResNet50	65.15M	30ms	56ms	93.65	79.07	60.96	92.91	40.61	91.98	74.14
ShuffleNet (s)	3.73M	12ms	14ms	87.32	61.21	57.32	91.03	32.31	91.13	69.83
ShuffleNet (m)	7.98M	15ms	25ms	91.14	75.46	56.7	92.92	32.50	90.90	72.09
ShuffleNet (l)	17.41M	21ms	39ms	96.72	78.3	61.66	92.79	40.90	92.62	73.91
EfficientNet (s)	22.69M	15ms	31ms	95.02	79.48	59.44	93.63	39.39	91.89	74.14
EfficientNet (m)	55.60M	19ms	36ms	96.21	79.89	61.9	93.92	41.07	92.79	75.44
EfficientNet (l)	120.31M	27ms	51ms	95.37	80.04	62.23	93.01	42.08	92.53	76.21

We conducted experiments using different backbone architectures to evaluate semantic segmentation accuracy and real-time performance. Two processing setups are considered: single LiDAR scan inference with a batch size of 1, and dual-sensor inference with a batch size of 2.

Models are assessed under a real-time constraint of 33.3 ms for dual inference. As shown in Table III and Figure 7, *EfficientNet (s)* achieves the best trade-off, reaching 74.14% mIoU, 31 ms latency, and 22.69M parameters. While *EfficientNet (l)* offers higher accuracy (76.21% mIoU), its latency exceeds the real-time threshold. Models based on *ResNet* and *ShuffleNet* generally perform worse in speed or accuracy.

Application-specific priorities also influence the selection of the model. In our case, accurate segmentation of the ground, person, and forklift classes is crucial. Lightweight models such as *ResNet18* and *ShuffleNet (s)* already perform well in these categories, achieving forklift IoUs between 85.51% and 88.93% and driveable ground IoUs of 92.32% and 91.03%, respectively. Higher-capacity models like those in the *EfficientNet* family significantly improve person segmentation, reaching up to 80.04% IoU.

The qualitative results in Figure 8 show the effectiveness of the model in real forklift operations within outdoor warehouse environments. The strong distinction between drivable and non-drivable ground is likely due to the integration of surface normal features, which capture terrain geometry effectively. Lane markings are segmented with high precision, aided by LiDAR reflectivity, which enhances visibility under varying environmental conditions. Dynamic objects such as people, forklifts, and vehicles are consistently detected, supporting robust obstacle awareness essential for collision avoidance and emergency response in complex scenarios.

V. CONCLUSIONS AND FUTURE WORK

In this work, we presented a novel semantic segmentation framework that leverages a dual high-resolution LiDAR setup specifically designed for autonomous forklifts operating in complex outdoor warehouse environments. Our approach demonstrated the ability to accurately segment safety-critical classes such as pedestrians, vehicles, and forklifts, as well as environmental characteristics crucial for navigation, including

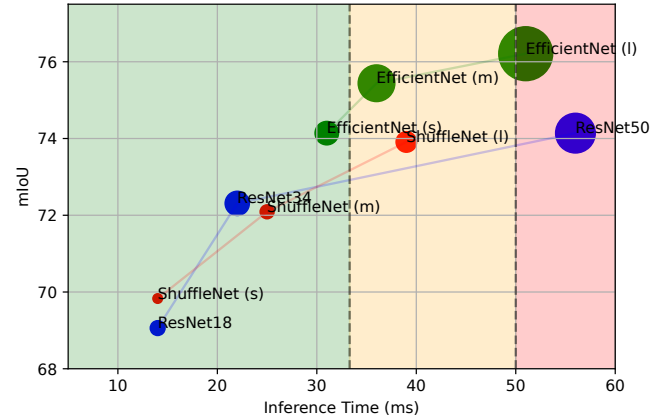


Fig. 7: **Model Comparison:** mIoU and inference time at single sensor inference. The size of the points sketch the number of parameters. The different zones show the real-time constraints.

drivable ground and lane markings. By combining forward-facing and downward-angled LiDAR sensors, our system achieved enhanced spatial coverage and robustness under real-world operational conditions. The lightweight segmentation method enables real-time inference, meeting the stringent timing requirements of autonomous forklift control loops.

Future work will focus on extending the current framework to incorporate dynamic scene understanding through temporal fusion, improving the tracking of moving obstacles, and handling occlusions more effectively. Additionally, integrating multi-modal sensor data such as camera imagery and radar could further enhance semantic perception under adverse weather or lighting conditions. Finally, deploying the system in a closed-loop autonomous navigation pipeline will provide comprehensive validation of its impact on task efficiency and safety in operational environments.

REFERENCES

- [1] Iñigo Alonso, Luis Riazuelo, Luis Montesano, and Ana Cristina Murillo. 3d-mininet: Learning a 2d representation from point clouds for fast and efficient 3d lidar semantic segmentation. *IEEE Robotics and Automation Letters*, 5:5432–5439, 2020. 4

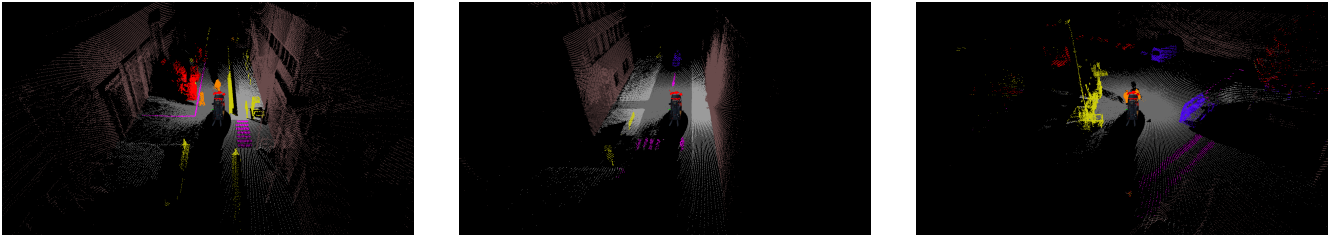


Fig. 8: **Qualitative Results:** Semantic segmentation of point clouds. Lane markings (purple) are clearly distinguishable due to the use of reflectivity measurements. Drivable and non-drivable ground are well separated, particularly in areas with elevation differences. Persons (red), cars (blue), and forklifts (orange) are segmented with sufficient accuracy to be easily recognizable.

- [2] Angelika Ando, Spyros Gidaris, Andrei Bursuc, Gilles Puy, Alexandre Boulch, and Renaud Marlet. Rangevit: Towards vision transformers for 3d semantic segmentation in autonomous driving. In *CVPR*, 2023. 2
- [3] Dimitrios Arapis, Milad Jami, and Lazaros Nalpantidis. Efficient human 3d localization and free space segmentation for human-aware mobile robots in warehouse facilities. *Frontiers in Robotics and AI*, 10:1283322, 10 2023. 2
- [4] J. Behley, M. Garbade, A. Milioto, J. Quenzel, S. Behnke, C. Stachniss, and J. Gall. SemanticKITTI: A Dataset for Semantic Scene Understanding of LiDAR Sequences. In *Proc. of the IEEE/CVF International Conf. on Computer Vision (ICCV)*, 2019. 1, 2
- [5] Hui-Xian Cheng, Xian-Feng Han, and Guo-Qiang Xiao. Cenet: Toward concise and efficient lidar semantic segmentation for autonomous driving. In *2022 IEEE International Conference on Multimedia and Expo (ICME)*, pages 01–06. IEEE, 2022. 2
- [6] Whye Kit Fong, Rohit Mohan, Juana Valeria Hurtado, Lubing Zhou, Holger Caesar, Oscar Beijbom, and Abhinav Valada. Panoptic nusenes: A large-scale benchmark for lidar panoptic segmentation and tracking. *arXiv preprint arXiv:2109.03805*, 2021. 2
- [7] Raphael Hagmanns, Peter Mortimer, Miguel Granero, Thorsten Luettel, and Janko Peterleit. Excavating in the wild: The goose-ex dataset for semantic segmentation. 2024. 2
- [8] Seyed Raef Hashemi, Seyed Sadegh Mohseni Salehi, Deniz Erdoğan, Sanjay P. Prabhu, S. Warfield, and Ali Gholipour. Tversky as a loss function for highly unbalanced image segmentation using 3d fully convolutional deep networks. *ArXiv*, abs/1803.11078, 2018. 4
- [9] Kaiming He, X. Zhang, Shaoqing Ren, and Jian Sun. Deep residual learning for image recognition. *2016 IEEE Conference on Computer Vision and Pattern Recognition (CVPR)*, pages 770–778, 2015. 4
- [10] chassis components ISO/TC 22/SC 33 Vehicle dynamics and driving automation systems testing. ISO 8855:2011 Road vehicles — Vehicle dynamics and road-holding ability — Vocabulary. Standard, International Organization for Standardization, Mar. 2011. 3
- [11] Peng Jiang and Srikanth Saripalli. Lidarnet: A boundary-aware domain adaptation model for lidar point cloud semantic. 2020. 2
- [12] Diederik P. Kingma and Jimmy Ba. Adam: A method for stochastic optimization. *CoRR*, abs/1412.6980, 2014. 4
- [13] Lingdong Kong, Youquan Liu, Runnan Chen, Yuexin Ma, Xinge Zhu, Yikang Li, Yuenan Hou, Yu Qiao, and Ziwei Liu. Rethinking range view representation for lidar segmentation. In *2023 IEEE/CVF International Conference on Computer Vision (ICCV)*, pages 228–240, 2023. 2
- [14] Xin Lai, Yukang Chen, Fanbin Lu, Jianhui Liu, and Jiaya Jia. Spherical transformer for lidar-based 3d recognition. In *CVPR*, 2023. 2
- [15] Tsung-Yi Lin, Piotr Dollár, Ross Girshick, Kaiming He, Bharath Hariharan, and Serge Belongie. Feature pyramid networks for object detection. In *2017 IEEE Conference on Computer Vision and Pattern Recognition (CVPR)*, pages 936–944, 2017. 4
- [16] Inc. Ouster. Ouster - scanning sensors oso - ultra-wide, 2023. Accessed at <https://ouster.com/products/scanning-lidar/os0-sensor/> on 2023-05-18. 2
- [17] Yancheng Pan, Biao Gao, Jilin Mei, Sibao Geng, Chengkun Li, and Huijing Zhao. Semanticpos: A point cloud dataset with large quantity of dynamic instances, 2020. 2
- [18] Hannes Reichert, Manuel Hetzel, Steven Schreck, Konrad Doll, and Bernhard Sick. Sensor equivariance by lidar projection images. In *2023 IEEE Intelligent Vehicles Symposium (IV)*, pages 1–6, 2023. 3
- [19] Hannes Reichert, Elijah Schüssler, Benjamin Serfling, Kerim Turacan, Konrad Doll, and Bernhard Sick. Semanticthab: A high resolution lidar dataset, Feb. 2025. 2
- [20] Hannes Reichert, Benjamin Serfling, Elijah Schüssler, Kerim Turacan, Konrad Doll, and Bernhard Sick. Real time semantic segmentation of high resolution automotive lidar scans, 2025. 2, 3
- [21] Steven Schreck, Hannes Reichert, Manuel Hetzel, Konrad Doll, and Bernhard Sick. Height change feature based free space detection. In *2023 11th International Conference on Control, Mechatronics and Automation (ICCMA)*, pages 171–176, 2023. 2, 3
- [22] Pei Sun, Henrik Kretschmar, Xerxes Dotiwalla, Aurelien Chouard, Vijaysai Patnaik, Paul Tsui, James Guo, Yin Zhou, Yuning Chai, Benjamin Caine, Vijay Vasudevan, Wei Han, Jiquan Ngiam, Hang Zhao, Aleksei Timofeev, Scott Ettinger, Maxim Krivokon, Amy Gao, Aditya Joshi, Yu Zhang, Jonathon Shlens, Zhifeng Chen, and Dragomir Anguelov. Scalability in perception for autonomous driving: Waymo open dataset. In *Proceedings of the IEEE/CVF Conference on Computer Vision and Pattern Recognition (CVPR)*, June 2020. 2
- [23] Mingxing Tan and Quoc Le. Efficientnetv2: Smaller models and faster training. In Marina Meila and Tong Zhang, editors, *Proceedings of the 38th International Conference on Machine Learning*, volume 139 of *Proceedings of Machine Learning Research*, pages 10096–10106. PMLR, 18–24 Jul 2021. 4
- [24] Haotian* Tang, Zhijian* Liu, Shengyu Zhao, Yujun Lin, Ji Lin, Hanrui Wang, and Song Han. Searching efficient 3d architectures with sparse point-voxel convolution. In *European Conference on Computer Vision*, 2020. 2
- [25] Ashish Vaswani, Noam Shazeer, Niki Parmar, Jakob Uszkoreit, Llion Jones, Aidan N Gomez, Ł ukasz Kaiser, and Illia Polosukhin. Attention is all you need. In I. Guyon, U. Von Luxburg, S. Bengio, H. Wallach, R. Fergus, S. Vishwanathan, and R. Garnett, editors, *Advances in Neural Information Processing Systems*, volume 30. Curran Associates, Inc., 2017. 4
- [26] Ignacio Vizzo, Tiziano Guadagnino, Jens Behley, and Cyrill Stachniss. Vdbfusion: Flexible and efficient tsdf integration of range sensor data. *Sensors*, 22(3), 2022. 3
- [27] Ignacio Vizzo, Tiziano Guadagnino, Benedikt Mersch, Louis Wiesmann, Jens Behley, and Cyrill Stachniss. KISS-ICP: In Defense of Point-to-Point ICP – Simple, Accurate, and Robust Registration If Done the Right Way. *IEEE Robotics and Automation Letters (RA-L)*, 8(2):1029–1036, 2023. 2
- [28] Yanbo Wang, Wentao Zhao, Chuan Cao, Tianchen Deng, Jingchuan Wang, and Weidong Chen. Sfpnet: Sparse focal point network for semantic segmentation on general lidar point clouds. In *European Conference on Computer Vision*, pages 403–421. Springer, 2024. 2
- [29] Xiaoyang Wu, Li Jiang, Peng-Shuai Wang, Zhijian Liu, Xihui Liu, Yu Qiao, Wanli Ouyang, Tong He, and Hengshuang Zhao. Point transformer v3: Simpler, faster, stronger. In *CVPR*, 2024. 2
- [30] Xiang Xu, Lingdong Kong, Hui Shuai, and Qingshan Liu. Fr-net: Frustum-range networks for scalable lidar segmentation. *ArXiv*, abs/2312.04484, 2023. 2
- [31] Xiangyu Zhang, Xinyu Zhou, Mengxiao Lin, and Jian Sun. Shufflenet: An extremely efficient convolutional neural network for mobile devices. In *2018 IEEE/CVF Conference on Computer Vision and Pattern Recognition*, pages 6848–6856, 2018. 4
- [32] Yiming Zhao, Lin Bai, and Xinming Huang. Fidnet: Lidar point cloud semantic segmentation with fully interpolation decoding. *2021 IEEE/RSJ International Conference on Intelligent Robots and Systems (IROS)*, pages 4453–4458, 2021. 2
- [33] Xinge Zhu, Hui Zhou, Tai Wang, Fangzhou Hong, Yuexin Ma, Wei Li, Hongsheng Li, and Dahua Lin. Cylindrical and asymmetrical 3d convolution networks for lidar segmentation. *arXiv preprint arXiv:2011.10033*, 2020. 2